SCIENCE CHINA
Information Sciences

• RESEARCH PAPER •

June 2021, Vol. 64 162402:1–162402:7
https://doi.org/10.1007/s11432-020-2959-6

Tuning the pinning direction of giant magnetoresistive sensor by post annealing process

Zhiqiang CAO[1,2], Yiming WEI[1,2], Wenjing CHEN[2], Shaohua YAN[1,2], Lin LIN[1], Zhi LI[1,2], Lezhi WANG[2], Huaiwen YANG[2*], Qunwen LENG[1,2,3*] & Weisheng ZHAO[1,2*]

[1]*Beihang-Geortek Joint Microelectronics Institute, Qingdao Research Institute, Beihang University, Qingdao* 266104*, China;*
[2]*Fert Beijing Institute, BDBC, School of Microelectronics, Beihang University, Beijing* 100191*, China;*
[3]*Goertek Inc., Weifang* 261031*, China*

Received 20 March 2020/Revised 7 June 2020/Accepted 15 June 2020/Published online 15 April 2021

Abstract The Internet of Things has created an increasing demand for giant magnetoresistive (GMR) sensor owing to its high sensitivity, low power-consumption and small size. A full Wheatstone bridge GMR sensor is fabricated on 6-inch wafers with an annealing process on patterned devices. It can be observed that GMR resistors could have different pinning directions in one wafer by magnetic resistance measurements and MATLAB simulations. The full Wheatstone bridge device shows a sensitivity of 2 mV/V/mT in a linear range of ±6 mT, and its angular response to the surrounding magnetic field is as low as 0.08 mT. These results demonstrate a new approach to high-sensitive and low-cost GMR sensors with a controllable post annealing process.

Keywords GMR sensor, full Wheatstone bridge, annealing, simulation

Citation Cao Z Q, Wei Y M, Chen W J, et al. Tuning the pinning direction of giant magnetoresistive sensor by post annealing process. Sci China Inf Sci, 2021, 64(6): 162402, https://doi.org/10.1007/s11432-020-2959-6

1 Introduction

Giant magnetoresistive (GMR) sensors have been widely used in industry and daily life since the GMR effect was discovered by Albert Fert [1] and Peter Grunberg [2] in the 1980s. In the magnetic sensing field, market demand has led to a wide range of applications, such as e-compass [3], nondestructive testing [4,5], biosensing [6]. Especially with the advent of the Internet of Things era, GMR sensors have provoked much attention owing to its high sensitivity, low power consumption and small size. As a good example in the consumer electronics and automotive industry, e-compass can track the location of mobile phones or vehicles in a sudden GPS signal loss [7]. Although the Hall sensor occupies a large part of e-compass market currently, the share of GMR-based magnetic sensors is growing owing to the urgent needs for sensors with higher sensitivity and smaller volume in the state-of-the-art application scenarios [8–10].

One of the major challenges faced by GMR-based sensors is how to meet the requirements of stabilization of thermal drifts since their operating ambient temperature varies meanwhile the GMR effect changes with temperature [11]. Wheatstone bridge configuration, as an effective way to solve the issue of thermal drift, consists of four active resistive elements, which have the same temperature coefficient ratio (TCR), and therefore it could have a null output when temperature drifts [12]. Meanwhile, the response of two adjacent resistive elements should be asymmetric to external fields to constitute a differential circuit, as shown in Figure 1(a) [13, 14].

There are several typical techniques to fabricate a full Wheatstone bridge based GMR sensor. A simple method is to assemble four identical resistive elements along with the opposite sensing directions, and then connect them via wire bonding [15]. However, this method may cause alignment errors, which is not conducive to mass production. To avoid this problem, fabricating the full Wheatstone bridge at one time

* Corresponding author (email: yanghw@buaa.edu.cn, lengqw@bhqditi.com, weisheng.zhao@buaa.edu.cn)

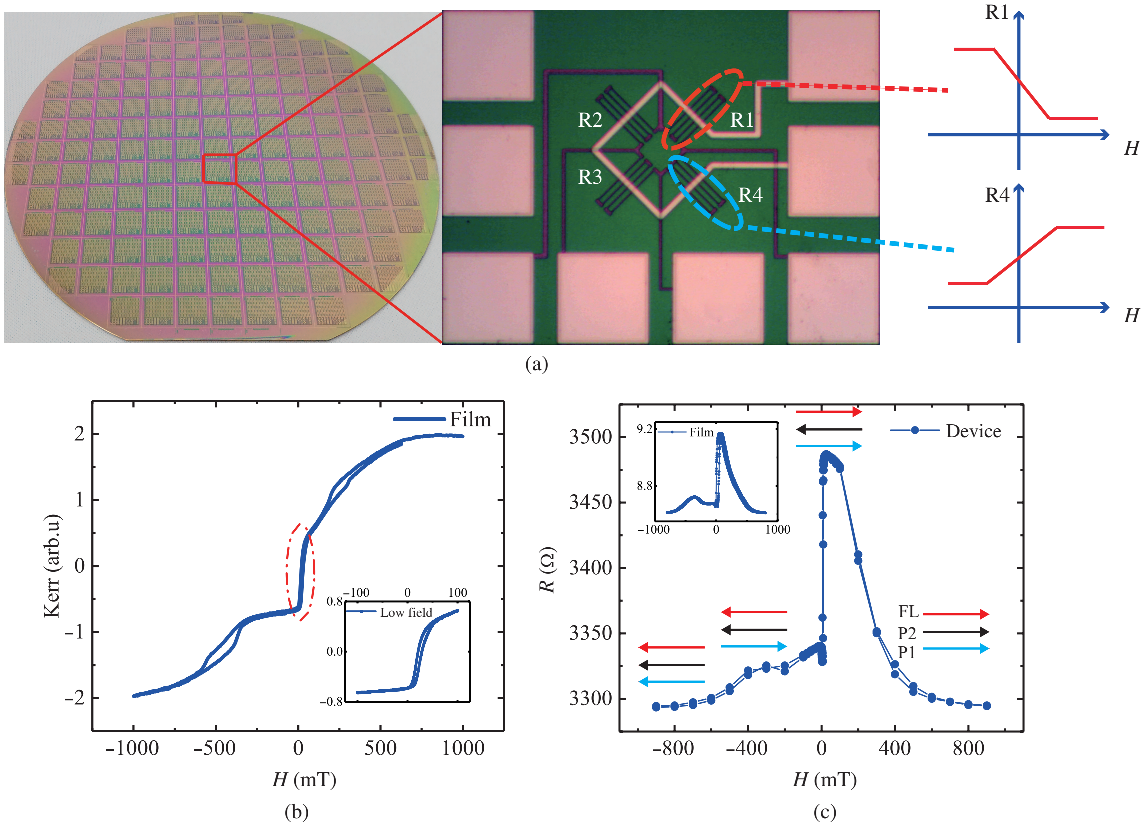

Figure 1 (Color online) (a) Image of a full 6-inch wafer and single device of Wheatstone bridge in the center field. (b) The Kerr loop of the full film measured at room temperature. (c) The *R*-*H* curve of the patterned device with the indicated magnetic directions of two pinned layers (P1, P2) and free layer (FL), respectively, and the inset shows the *R*-*H* curve of the full film.

is a good option. Many researchers have exploited various new processes. One method is to form two opposite pinning direction of GMR films on the same wafer by changing the synthetic antiferromagnetic (SAF) structures with two steps deposition, and then fabricate devices [16]. This method can solve the deferential circuit problem, but it will increase the cost during the film deposition process. Another approach is to anneal the patterned devices by local laser heating and magnetic field, which is considered to be a popular candidate method [17]. However, the inefficiency of the laser heating process restrains the throughput of mass production. In our previous research, a concise one-time post annealing process has been demonstrated to fabricate the full bridge GMR sensor [18]. In this paper, we implanted these processes on 6-inch wafers, studied the pinning directions of the full bridge sensor, and gave a detailed simulation proof, to prove that post annealing process is a promising method for mass production.

2 Materials and methods

A bottom-pinned multilayer stack Ta(5.0 nm)/NiFe19(2.0 nm)/IrMn80(7.5 nm)/CoFe10(2 nm)/Ru(0.85 nm)/CoFe30(2.1 nm)/CuO(1.9 nm)/CoFe30(1.0 nm)/NiFe19(2.0 nm)/Cu(1.0 nm)/Ta(3.0 nm) is deposited on thermally oxidized Si substrates by a Singulus magnetron-sputtering system. The film is patterned to devices by lift-off and etching processes. Lithography and etching were performed with Nikon I10D stepper and ion beam etch (IBE). The details of fabrication processes can be found in the study of other researchers [19]. The patterned wafer was then annealed in a high vacuum Futek furnace at 270°C under 1 T magnetic field which is set along the X axis for 1 h to define its pinning direction. The key to this post annealing process is the design of each transducer in the Wheatstone bridge, as shown in Figure 1(a). The angle of transducers between the annealing magnetic field was $-45°$ and $45°$, respectively. Each transducer was designed as 2 µm × 50 µm and 4 transduces connected in serials to form a bridge element. By tuning the annealing condition, it could have a Y-direction field response as in Figure 1(a).

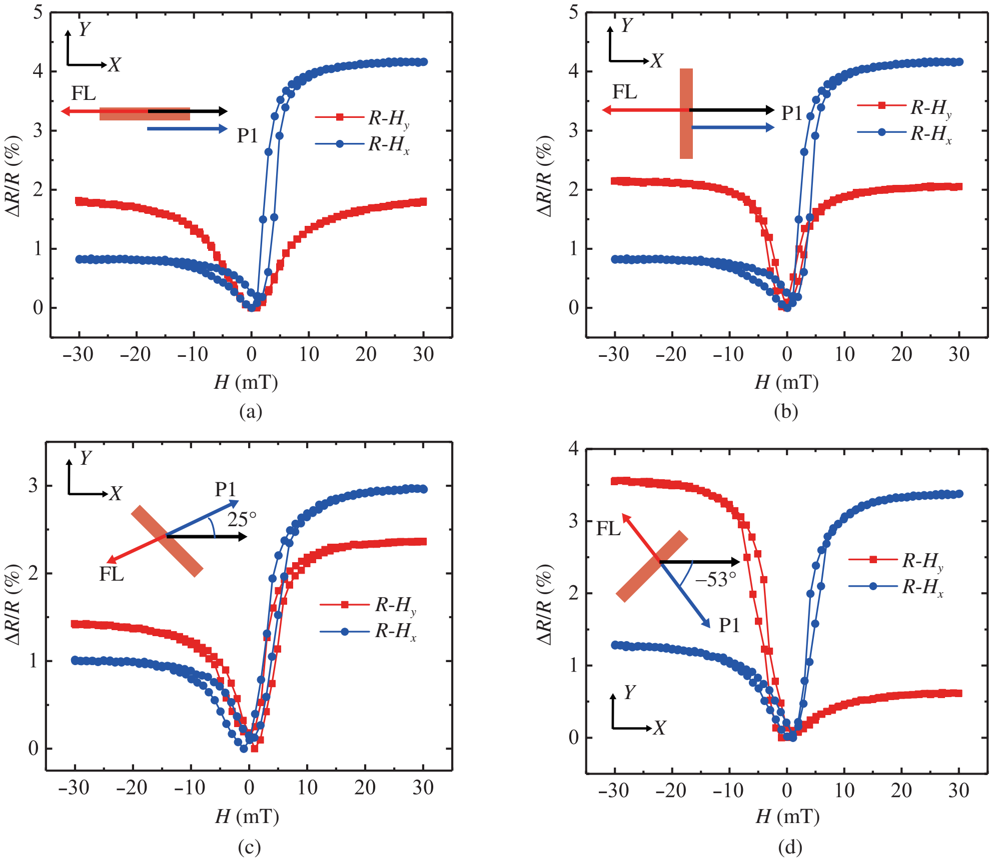

Figure 2 (Color online) (a) The R-H loop of a GMR transducer along the annealing direction. (b) The R-H loop of a GMR transducer perpendicular to the annealing direction. (c) The R-H loop of a GMR transducer with an angle of -45° to the annealing direction, and (d) the R-H loop of a GMR transducer with an angle of 45° to the annealing direction.

The magnetic properties of full films are characterized by the magneto-optical Kerr effect (MOKE) system and a vibrating sample magnetometer (VSM). The change of resistance and voltage with an external field ($H_{\rm ext}$) is measured on a four-probe platform. The R-H curves of GMR transducers are measured by tracking the voltage at a fixed bias current of 1 μA, and V-H curves of Wheatstone bridges are characterized under a bias voltage of 1 V at room temperature. The angular response to the ambient magnetic field is measured by a rotation station.

3 Results and discussion

Figure 1(b) shows the in-plane magnetization curve of the film under $H_{\rm ext}$ applied along the X-axis. In the stack, the first pinned layers (P_1), the second pinned layer (P_2), and the free layer (FL) played important roles when the magnetic field changes. The film exhibits an exchange coupling field of about 300 mT, indicating that P_1 has good performance. Here, P_1 and P_2 are antiferromagnetically coupled when the thickness of Ru is 0.85 nm. P_2 and FL are ferromagnetically coupled and the interlayer coupling field ($H_{\rm in}$) is about 2 mT. As shown in the inset of Figure 1(b), the R-H curve of full film is $R_{AP} = 22.94\ \Omega/\square$ and $R_P = 21.63\ \Omega/\square$; i.e., R_{AP} and R_P is the sheet resistance of the film when moments of P_2 and FL are aligned in antiparallel and parallel ways, respectively. The GMR ratio $\Delta R/R = (R_{AP} - R_P)/R_P \times 100\%$ [20] is 6.05%. The R-H curve of a Wheatstone bridge element under the same $H_{\rm ext}$ is shown in Figure 1(c) and its GMR ratio reaches about 4.7%. The reduction in GMR ratio is due to contact resistance and damages at the edges of devices during fabrication [21].

Figure 2(a) is about the R-H_y curve of a 0° design transducer which shows symmetry behavior as the magnetic field changes from negative to positive, meaning that H_y is perpendicular to P_1. And R-H_x shows the largest magnetoresistance (MR) with maximum magnetic hysteresis. It is concluded that P_1 is along with the annealing direction of X axis. At zero field, the curve is at its lowest point, meaning that

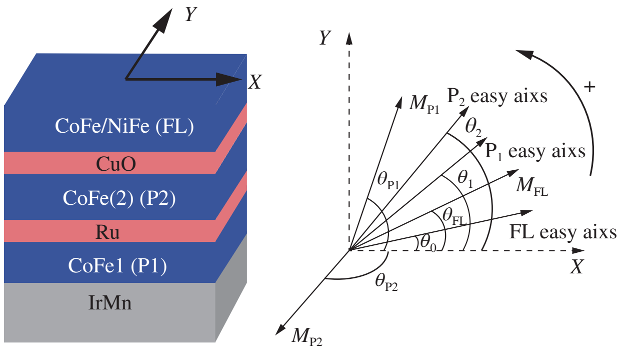

Figure 3 (Color online) The simplified film stack and schematic geometry of the magnetization M in each layer of transducer.

P_2 and FL are ferromagnetically coupled. Figure 2(b) is the R-H curve of a 90° design transducer which is the same as 0° design, showing that P_1 direction is along the annealing magnetic field. Figure 2(c) is a −45° design transducer, and R-H_x and R-H_y loops show similar behaviors which indicates that the P_1 direction exhibits a deflection angle with the annealing field. To find the accurate deflection angle, we measure the R-H_y loop in different directions by rotating the device to get a symmetric R-H_y loop which means that H_y is perpendicular to P_1 direction, and finally the angle is obtained to be 25°. In the 45° design GMR transducers, the pinning direction is determined in the same way, and its angle is found to be −53°. By comparing 45° and −45° design GMR transducers, it can be found that their $\mathrm{d}R/\mathrm{d}H_y$ exhibited opposite signs, which serve as two adjacent elements of a Wheatstone bridge. And the signs of $\mathrm{d}R/\mathrm{d}H_x$ are in the same, meaning that the sensitive axis of the Wheatstone bridge is the Y direction.

To confirm that the pinned directions of magnetic layers are accurately measured, a simulation was performed on MATLAB, based on Stoner-Wohlfarth coherent rotation model [22, 23]. The calculating energy in the sensor model includes Zeeman energy, anisotropy energy, interlayer coupling energy between ferromagnetic layers and exchange coupling energy between P_1 and antiferromagnetic layer. The energy per unit area can be expressed as

$$E = E_{\rm FL} + E_{\rm P1} + E_{\rm P2}, \tag{1}$$

where $E_{\rm FL}$ is the energy of FL, $E_{\rm P1}$ and $E_{\rm P2}$ are the energy of P1 and $\rm P_2$, respectively. Figure 3 is the schematic geometry of the magnetization M in each layer of spin valve transducer. For FL, the energy is given by

$$E_{\rm FL} = -M_{\rm FL}\cdot H_{\rm ext} - M_{\rm FL}\cdot H_{\rm in} + 2\pi\frac{M_{\rm FL}^2 t_{\rm FL}}{\rm w}\sin^2(\theta_{\rm FL}-\theta_0) + \frac{1}{2}M_{\rm FL}H_{\rm kFL}\sin^2(\theta_{\rm FL}-\theta_0), \tag{2}$$

where the first term is Zeeman energy, the second term describes the interlayer coupling energy, the third term is the shape anisotropy energy and the last term is induced anisotropy energy. In this equation, $M_{\rm FL}$ is the magnetization of FL, $t_{\rm FL}$ is the thickness of FL, w is the width of the device, $H_{\rm kFL}$ is the induced anisotropy field of FL, $\theta_{\rm FL}$ is the angle between $M_{\rm FL}$ and the X direction. And θ_0 is the angle between the easy axis (e.a.) of FL and the X direction. In $\rm P_1$, the energy is expressed as

$$E_{\rm P1} = -M_{\rm P1}\cdot H_{\rm ext} - M_{\rm P1}\cdot H_{\rm ex} + 2\pi\frac{M_{\rm P1}^2 t_{\rm P1}}{\rm w}\sin^2(\theta_{\rm P1}-\theta_1) + \frac{1}{2}M_{\rm P1}H_{\rm kP1}\sin^2(\theta_{\rm P1}-\theta_1), \tag{3}$$

where $M_{\rm P1}$ is the magnetization of $\rm P_1$, $t_{\rm P1}$ is the thickness of $\rm P_1$, $H_{\rm kP1}$ is the induced anisotropy field of $\rm P_1$, $\theta_{\rm P1}$ is the angle between $M_{\rm P1}$ and X direction and θ_1 is the angle between e.a. of $\rm P_1$ and X direction. Similarly, the energy expression of $\rm P_2$ is as follows:

$$E_{\rm P2} = -M_{\rm P2}\cdot H_{\rm ext} + 2\pi\frac{M_{\rm P2}^2 t_{\rm P2}}{\rm W}\sin^2(\theta_{\rm P2}-\theta_2) + \frac{1}{2}M_{\rm P2}H_{\rm kP2}\sin^2(\theta_{\rm P2}-\theta_2) + M_{\rm P2}\cdot H_{\rm P1P2}, \tag{4}$$

where the last term is the coupling energy of $\rm P_1$ and $\rm P_2$. $M_{\rm P2}$, $t_{\rm P2}$, $H_{\rm kP2}$, $\theta_{\rm P1}$ and θ_2 have the same definition as that in (3) and $H_{\rm P1P2}$ is the coupling field between $\rm P_1$ and $\rm P_2$.

Based on the principle of energy minimization, we can deduce the formula $\Delta R/R = \frac{1}{2}\mathrm{MR}[1-\cos(\theta_{\rm FL}-\theta_{\rm P2})]$, where MR is the maximum magnetoresistance of the sensor. Figure 4(a) shows a −45° design GMR transducer and Figure 4(c) is about a 45° design GMR transducer, and both transducers were measured

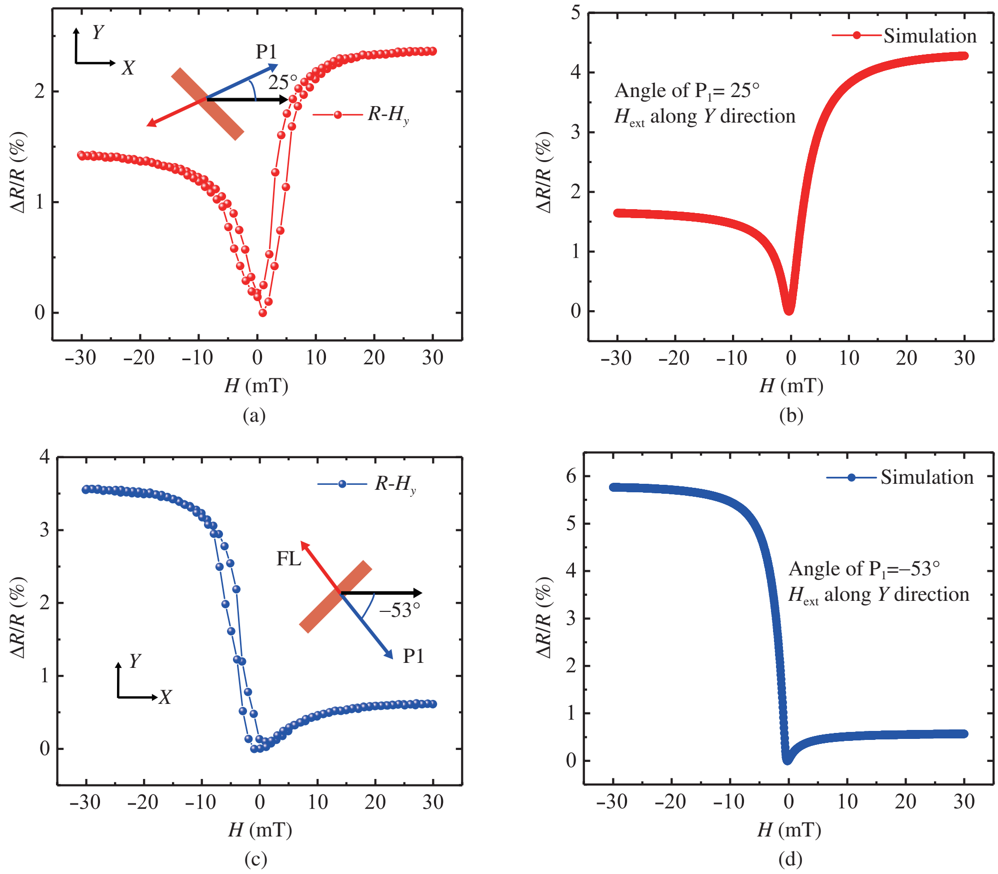

Figure 4 (Color online) (a) The *R*-*H* curve of $-45°$ GMR transducer under Y direction $H_{\rm ext}$. (b) MR-H curve of a GMR transducer under Y direction $H_{\rm ext}$ where θ_1 is set to 25° and θ_2 is set to $-155°$ to match the measured pinning direction. (c) 45° GMR transducer result and (d) the correspondent simulation with $\theta_1 = -53°$ and and $\theta_2 = 127°$. *R*-*H* loop calculated with the following parameters: MR $= 6.05\%$, $M_{\rm FL} = 1060$ emu/cm^3, $M_{\rm P1} = 1580$ emu/cm^3, $M_{\rm P2} = 1850$ emu/cm^3, $H_{\rm in} = 2$ mT, $H_{\rm kFL} = 1$ mT, $H_{\rm kP1} = 3$ mT, $H_{\rm kP2} = 3$ mT, $H_{\rm ex} = 200$ mT, $H_{\rm P1P2} = 500$ mT, $t_{\rm FL} = 3 \times 10^{-7}$ cm, $t_{\rm P1} = 2 \times 10^{-7}$ cm, $t_{\rm P2} = 2.1 \times 10^{-7}$ cm and $W = 2 \times 10^{-4}$ cm.

and analyzed under Y direction field. Figures 4(b) and (d) are the corresponding simulated curves. In Figure 4(b), the simulation parameters were set to be the same as measurement results, i.e., $\theta_0 = -45°$, $\theta_1 = 25°$ and $\theta_2 = -155°$, MR $= 6.05\%$, $M_{\rm FL} = 1060$ emu/cm^3, $M_{\rm P1} = 1580$ emu/cm^3, $M_{\rm P2} = 1850$ emu/cm^3, $H_{\rm in} = 2$ mT, $H_{\rm kFL} = 1$ mT, $H_{\rm kP1} = 3$ mT, $H_{\rm kP2} = 3$ mT, $H_{\rm ex} = 200$ mT (measured by a Ta(3.0 nm)/Ru(3.0 nm)/IrMn(7.5 nm)/CoFe10(2.1 nm)/Ta(2.0 nm) multilayer), $H_{\rm P1P2} = 500$ mT (measured by a Ta(3.0 nm)/Ru(3.0 nm)/CoFe10(2.1 nm)/Ru(0.85 nm)/CoFe30(2.0 nm)/Ta(2.0 nm) structure), $t_{\rm FL} = 3 \times 10^{-7}$ cm, $t_{\rm P1} = 2 \times 10^{-7}$ cm, $t_{\rm P2} = 2.1 \times 10^{-7}$ cm and $W = 2 \times 10^{-4}$ cm. It shows that the simulated R-H_y curve is similar to the measured curve. In Figure 4(d), the simulated parameters $\theta_0 = 45°, \theta_1 = -53°$ and $\theta_2 = 127°$ are changed and the others remain the same. By comparing Figures 4(c) and (d), the trend between experimental and simulation results matches each other well, despite a little mismatch in the actual behaviors, for the stray field and edge effect are not considered. But the simulated trend has proved the measurement to determine magnetic direction is reliable.

The GMR transducers could have two different pinning directions owing to shape anisotropy and stray field of the patterned device. Annealing process includes two stages. The first stage includes annealing under a field of 1 T during 1 h at a temperature of 270°C. This temperature exceeds the blocking temperature for the antiferromagnet IrMn80. In this stage, moments of pinning and pinned layer are normalized to the direction of the external magnetic field. The second stage is to remove the external magnetic field and cool it down. In this stage, with the help of stray field and shape anisotropy, the magnetization of pinning layers turns to the lowest energy state as we simulate, and their rotation direction is opposite. After the devices cool down to blocking temperature, the directions then are fixed with the help of exchange coupling between IrMn80 and CoFe10.

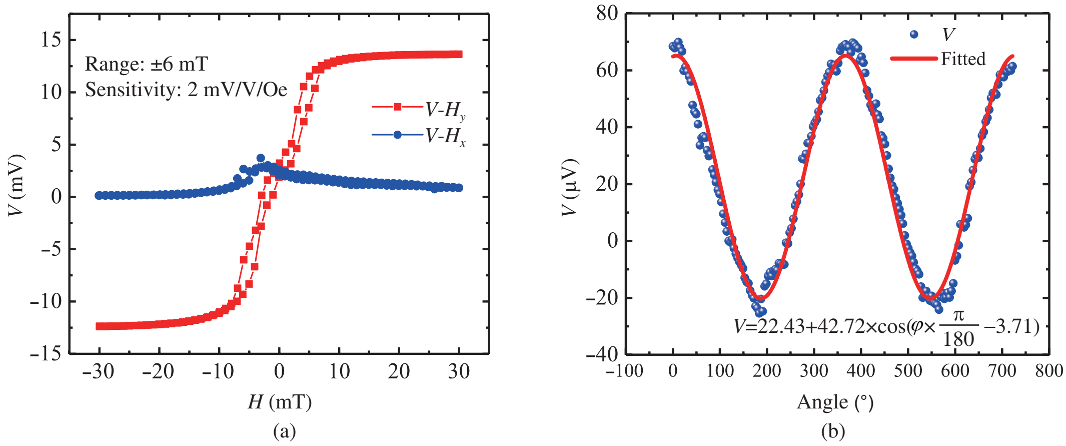

Figure 5 (Color online) (a) The output of bridge under a 1 V bias voltage and (b) the angular dependence output of full Wheatstone bridge under an environmental magnetic field.

In Figure 5(a), the output of the full bridge sensor is measured under a 1 V bias voltage by sweeping the external field in a range of ±30 mT. The sensor has a linear response to the external field along the Y-axis and has a sensitivity of up to 2 mV/V/mT within the linear range of ±6 mT. When the external field is along the X direction, the output of the sensor is approximate to zero, meaning that it is insensitive to this field and the hump is near zero field, for P_1 of 45° and −45° design GMR transducers are not orthogonal well. It has a linear output in the Y direction, illustrating that this bridge can be a magnetic field sensor along the Y direction. Figure 5(b) is an angular dependence output of the device under an environmental magnetic field which is about 0.08 mT. The output voltage has a good cosine relation to the rotation angle which is $V = 22.43 + 42.72 \times \cos(\varphi \times \frac{\pi}{180} - 3.71)$ (μV). The voltage offset about 22.43 μV is due to an unbalanced Wheatstone bridge caused by lithography or etching. And phase shift is introduced when the sensor is put on the measurement platform. Using the highest slope of the fitted curve to stand the angle sensitivity of the sensor, a value of 0.75 μV/° can be derived. This performance shows the sensor is a good candidate for the e-compass application.

4 Conclusion

In conclusion, a full Wheatstone bridge GMR sensor is fabricated on 6-inch wafers with annealing process on patterned devices. P_1 of 4 kinds of GMR transducers design were measured, demonstrating that it could have different pinning directions in one wafer. A MATLAB simulation of each layer magnetization has been performed and proved that the measurement of P_1 is proper. The sensitivity of this sensor reached 2 mV/V/mT in a linear range of ±6 mT which can sense the environmental magnetic field around 0.08 mT. This method makes it possible to produce a full Wheatstone bridge structure sensor at a lower cost and can be a promising solution for mass production.

Acknowledgements The work was financially supported by National Natural Science Foundation of China (Grant No. 61627813), International Collaboration Project B16001, and VR Innovation Platform from Qingdao Science and Technology Commission.

References

1 Baibich M N, Broto J M, Fert A, et al. Giant magnetoresistance of (001)Fe/(001)Cr magnetic superlattices. Phys Rev Lett, 1988, 61: 2472–2475
2 Binasch G, Grünberg P, Saurenbach F, et al. Enhanced magnetoresistance in layered magnetic structures with antiferromagnetic interlayer exchange. Phys Rev B, 1989, 39: 4828–4830
3 Trinh X T, Jeng J T, Lu C C, et al. Miniature tri-axis magnetometer with in-plane GMR sensors. IEEE Trans Magn, 2017, 53: 1–4
4 Bernieri A, Ferrigno L, Laracca M, et al. Eddy current testing probe based on double-coil excitation and GMR sensor. IEEE Trans Instrum Meas, 2019, 68: 1533–1542
5 Ye C, Huang Y, Udpa L, et al. Differential sensor measurement with rotating current excitation for evaluating multilayer structures. IEEE Sens J, 2016, 16: 782–789
6 Ravi N, Rizzi G, Chang S E, et al. Quantification of cDNA on GMR biosensor array towards point-of-care gene expression analysis. Biosens Bioelectron, 2019, 130: 338–343
7 Freitas P P, Ferreira R, Cardoso S. Spintronic sensors. Proc IEEE, 2016, 104: 1894–1918
8 Guedes A, Macedo R, Jaramillo G, et al. Hybrid GMR sensor detecting 950 pT/sqrt(Hz) at 1 Hz and room temperature. Sensors, 2018, 18: 790

9 Zhu C, Zhang L, Geng J W, et al. A micro-array bio detection system based on a GMR sensor with 50-ppm sensitivity. Sci China Inf Sci, 2017, 60: 082403
10 Wang L, Hu Z, Zhu Y, et al. Electric field-tunable giant magnetoresistance (GMR) sensor with enhanced linear range. ACS Appl Mater Interfaces, 2020, 12: 8855–8861
11 Ouyang Y, Wang Z, Zhao G, et al. Current sensors based on GMR effect for smart grid applications. Sens Actuat A-Phys, 2019, 294: 8–16
12 Swastika P E, Antarnusa G, Suharyadi E, et al. Biomolecule detection using Wheatstone bridge giant magnetoresistance (GMR) sensors based on CoFeB spin-valve thin film. J Phys-Conf Ser, 2018, 1011: 012060
13 Giebeler C, Adelerhof D J, Kuiper A E T, et al. Robust GMR sensors for angle detection and rotation speed sensing. Sens Actuat A-Phys, 2001, 91: 16–20
14 Li L, Mak K Y, Leung C W, et al. Detection of 10-nm superparamagnetic iron oxide nanoparticles using exchange-biased GMR sensors in Wheatstone bridge. IEEE Trans Magn, 2013, 49: 4056–4059
15 Lu C C, Liu Y T, Jhao F Y, et al. Responsivity and noise of a wire-bonded CMOS micro-fluxgate sensor. Sens Actuat A-Phys, 2012, 179: 39–43
16 Jeng J T, Trinh X T, Hung C H, et al. Quasi-static current measurement with field-modulated spin-valve GMR sensors. Sensors, 2019, 19: 1882
17 Berthold I, Müller M, Ebert R, et al. Selective realignment of the exchange biased magnetization direction in spintronic layer stacks using continuous and pulsed laser radiation. In: Proceedings of SPIE, 2014. 8967: 89671F
18 Yan S, Cao Z, Guo Z, et al. Design and fabrication of full Wheatstone-bridge-based angular GMR sensors. Sensors, 2018, 18: 1832
19 Reig C, Cubells-Beltrán M D, Muñoz D R. Magnetic field sensors based on giant magnetoresistance (GMR) technology: applications in electrical current sensing. Sensors, 2009, 9: 7919–7942
20 Vedyayev A, Dieny B, Ryzhanova N, et al. Angular dependence of giant magnetoresistance in magnetic multilayered structures. Europhys Lett, 1994, 25: 465–470
21 Peng X, Wakeham S, Morrone A, et al. Towards the sub-50nm magnetic device definition: ion beam etching (IBE) vs plasma-based etching. Vacuum, 2009, 83: 1007–1013
22 Labrune M, Kools J C S, Thiaville A. Magnetization rotation in spin-valve multilayers. J Magn Magn Mater, 1997, 171: 1–15
23 Qian Z, Bai R, Yang C, et al. Effective anisotropy field in the free layer of patterned spin-valve resistors. J Appl Phys, 2011, 109: 103904